# Supplementary Information: Experimental demonstration of scalable quantum key distribution over a thousand kilometers

**A. Aliev, V. Statiev, I. Zarubin, N. Kirsanov, D. Strizhak, A. Bezruchenko, A. Osicheva, A. Smirnov, M. V. Yarovikov, A. D. Kodukhov, V. Pastushenko, M. Pflitsch, and V. Vinokur**

**Terra Quantum AG**

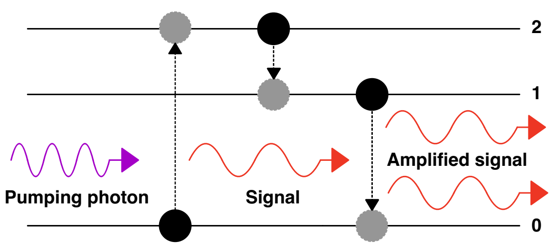


**Suppl Figure 1 | Transitions in the erbium-doped fiber system.** Because of the pump absorption, photons from the ground state move to the short-living (about 20 $\mu$s) state. Then photons transit to the first excited state and stay there for about 1 ms. This way, we keep the inverse population of erbium ions. The transition from state 1 leads to the coherently synchronized photons emission.

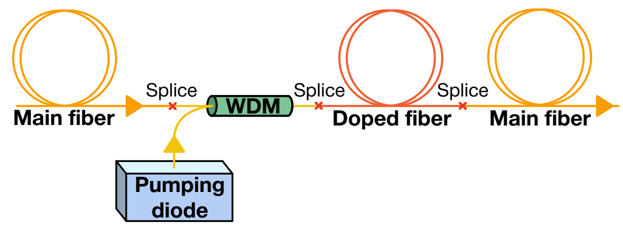


**Suppl Figure 2 | The scheme of the bidirectional (Terra Quantum AG-made) amplifier.** Wavelength-division multiplexing (WDM) system on its input unites the informational signal from the optical line and pump from the diode and releases them together in an active fiber section which is further connected with the main fiber.

## NOTE 1. Amplifiers

Due to natural losses of photons, there is a fundamental limit to long-distance quantum communication. The well-known PLOB-repeaterless bound, see Ref. [12] of the main text, emerges due to the exponential signal decay over distance. It imposes restrictions for creating a wide-spread quantum network. That is the main reason why we should use quantum repeaters which gain incoming signals and compensate for losses in the line. As an amplifying factor in standard telecommunication routes, the active fiber is used. The most widespread amplifiers are the Erbium-doped fiber amplifiers (EDFA), see Ref. [47] of the main text, where each erbium ion could be considered as a third-level system depicted in SI Fig. 1.

We emphasize that our Terra Quantum AG-made optical amplifiers based on the EDFA principle are bidirectional and have no optical isolators, filters, or detectors. Such construction had previously been used in works [1–3] and gives us an additional opportunity to control line via the OTDR. The amplifiers consist of a pumping diode and active fiber which are connected via the wavelength-division multiplexing (WDM) represented in Fig. 2. The system of WDM allows the transmission of signals with different wavelengths onto a single optical fiber at the same time.

Despite we removed isolators from the amplifiers, the line still can stay stable because the amplifiers are spaced far apart and the reflection back does not overcome lasing generation threshold. In the presented 1032-km line we use 19 such amplifiers separated from each other by 50 km. It is important to note here the peak of the EDFA spectrum lies at the wavelength 1530 nm, therefore, due to removing filters from the amplifiers, we chose 1530 nm as the main informational wavelength.

Despite we removed isolators from the amplifiers, the line still can stay stable because the amplifiers are spaced far apart and the reflection back does not overcome lasing generation threshold. In the presented 1032-km line we use 19 such amplifiers separated from each other by 50 km. It is important to note here the peak of the EDFA spectrum lies at the wavelength 1530 nm, see SI Fig. 3, therefore, due to removing filters from the amplifiers, we chose 1530 nm as the main informational wavelength.

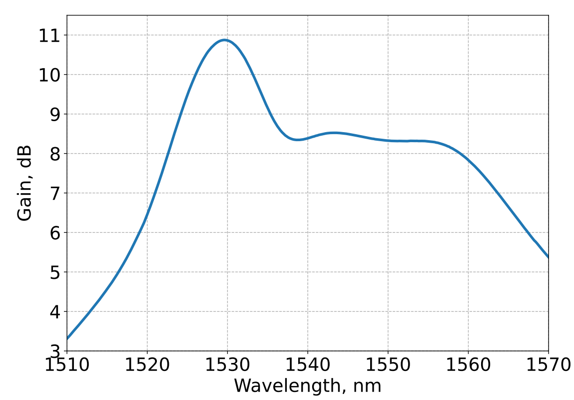


**Suppl Figure 3 | Amplification spectrum of magistral amplifiers**. The amplification peak for the amplification coefficient of about 10 dB is at 1530.33 nm.

Eavesdroppers could try to attack our amplifiers by increasing the gain factor and stealing extra photons. However, the amplifiers work in the regime with almost maximal pumping. It means that we need a minimum number of excited ions to achieve the target amplification of the incoming signal.

## NOTE 2. The splice losses

### Mode losses caused by splice joint

It is usually believed that at present the low-loss splices can be done only in a laboratory, but due to the constantly improving splicing equipment, it becomes useful to measure the loss value for splices done on some commercial device. First of all, we need to consider the part of the optical line with one splice joint, see Fig. 4. It divides this segment of the fiber into two parts. Let $T$, $R$, and $S$ be the transmission, reflection, and other loss coefficients, respectively. They satisfy the equation

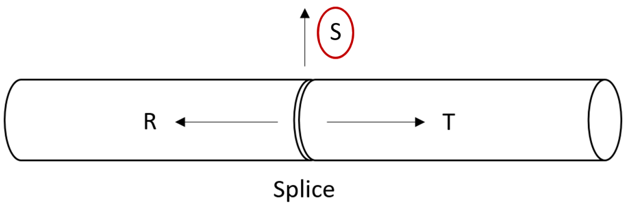


**Suppl Figure 4** | Splice joint in an optical line.

$$T + R + S = 1. \tag{1}$$

Since the reflected signal continues to propagate through the waveguide, it is inaccessible to a potential eavesdropper. Thus, the $S$ coefficient is of interest for the calculation of the signal leakage and, therefore, it is necessary to know the values of $T$ and $R$. It is technically easier, to begin with measuring the value of $T$. The corresponding experiment scheme is shown in Fig. 5. Each iteration is carried out in two steps. First, there is a part of a single-mode fiber, which is connected to a laser source on one side and to an optical power meter on the other side. After that, the output power data are collected for two minutes and averaged. The stability of the laser source power was also checked. The drift of the average value was about 0.01% in 8 minutes, and this value decreases later as the laser gradually reaches a stable regime. In the second step, the fiber is broken, spliced, and the average output power is measured in a similar way. This data becomes the reference for the next iteration (fiber is broken near the first joint, spliced, and the transmittance of the second splice will be measured with respect to the waveguide with one splice, etc.) The length of the single-mode fiber section used in this experiment is no more than 10 meters, so its attenuation can be neglected.

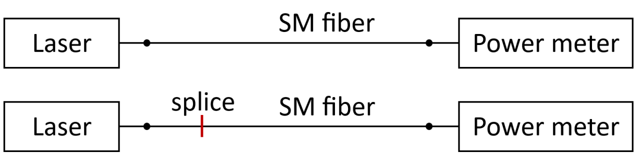


**Suppl Figure 5** | Experiment to measure the splice joint transmittance.

As a result, the transmittance of each splice joint can be calculated with the formula

$$T = \frac{P_{\text{step 2}}}{P_{\text{step 1}}}. \tag{2}$$

And, consequently, the losses on Bob's side are

$$R + S = 1 - \frac{P_{\text{step 2}}}{P_{\text{step 1}}}. \tag{3}$$

The results of measuring $S + R$ for the Fujikura 86S fusion splicer in the SM Auto regime give the best value of 0.48 % and the average value of $(0.65 \pm 0.28)$ %. It can be seen from the tabular data that the average laser source power change over 8 minutes is much less than the best loss value. Therefore, the source can be considered as being stable within one experimental iteration with good accuracy. Moreover, the random error of the average loss values exceeds the value of the average power change over 8 minutes by more than 10 times. Consequently, the contribution of the laser power drift to the error of the average splice loss value is negligibly small and almost all of it consists of random splicing procedure errors, like the roughness of fiber cleave, splicing regime errors, and similar ones.

Now, in order to calculate the $S$ value, it is necessary to investigate the reflected signal. The scheme of the corresponding experiment is shown in Fig. 6. The laser signal passes through a 50/50 beamsplitter and then half of it propagates along a piece of fiber. The optical signal power is measured at the splitter output which is adjacent to the laser output. The difference between the two experimental stages is in the presence of a splice joint in the studied piece of fiber in the second stage.

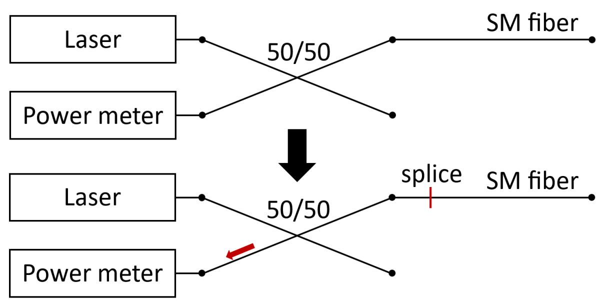


**Suppl Figure 6** | Reflection coefficient evaluation.

In the first stage, interference with a range from 1 to 51 nW was registered by a power meter. This signal comprises reflections from the joint between the splitter and fiber segment and reflections from the splitter and fiber ends. In the second stage, the range of interference was from 4 to 82 nW. Therefore, with the known value of the incident power $P_{\text{in}}$ propagating at the first stage through the fiber segment (it is almost equal to the optical power right before the splice joint at the second stage), the reflection coefficient can be estimated by the formula

$$R \leq \frac{2(P^{(2)}_{\max} - P^{(1)}_{\max})}{P_{\text{in}}}, \tag{4}$$

where $P^{(j)}_{\max}$ is the maximum value of reflected signal power measured at the $j$-th stage. For $P_{\text{in}}$=10 mW, $R \leq 6.2 \times 10^{-6} < 10^{-5}$. Thus, even the upper estimate of $R$ is much less than the sum $S + R$, which allows us to conclude that almost all the power lost for Bob's side does not remain in the reflected signal. Or, in a mathematical form, $S + R \approx S$, $S \approx 1 - T$. As a result, at present, even an automatic program on the common commercial splicing device allows achieving a loss value less than 1% on average and around 0.5% in good cases.

### Emitted power

Nevertheless, not all optical power lost on the splice joint is scattered into the external environment and can be collected by an eavesdropper eventually. For quantitative research of the emitted power fraction, the experiment, a schematic picture of which is given in Fig. 7, was carried out for the three splices with different loss values $S$. In this experiment,

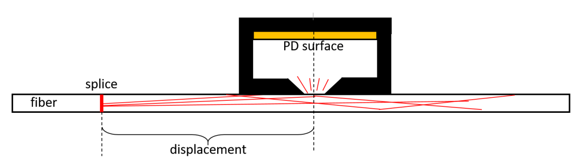


**Suppl Figure 7** | Measurement scheme.

a photodetector with a special cap which increases the spatial resolution is moved along the fiber and the optical power is recorded during the transmission of the laser radiation through the splice joint. The experimental data represent the emitted power dependence on the detector's center displacement relative to the splice. The graph example is given below in Fig. 8. By integrating the function plotted in this graph and taking into account that at each point only a part of the radiation is collected by photodetector, it is possible to calculate the integral value of the emitted optical power $P_e$. As a result, it turns out to be around 1/4 of the $S$ value on average, as presented in Table 1.

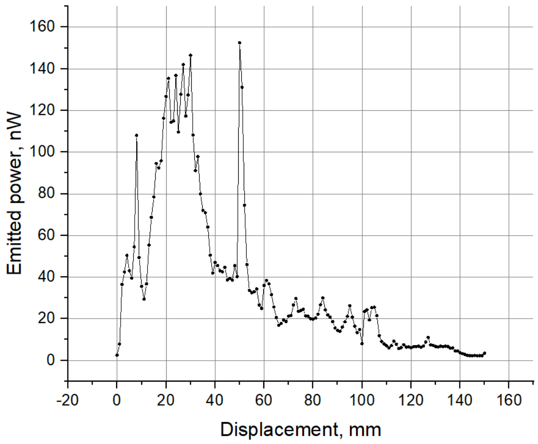


**Suppl Figure 8** | Emitted power distribution for splice with $S = 0.55\%$.

| № of splice | $P_{in}$, mW | $S$, % | $\tilde{S} = P_e/P_{in}$, % | $\tilde{S}/S$ |
|---|---|---|---|---|
| 1 | 18.38 | 0.65 | 0.162 | 0.25 |
| 2 | 18.26 | 0.33 | 0.095 | 0.29 |
| 3 | 18.20 | 0.55 | 0.132 | 0.24 |
| Average: | | | | $0.26 \pm 0.03$ |

**Suppl Table 1** | Power emitted and collected.

It is worth noticing here, that all the measurements were done on splices without any additional protection, the example of which is shown below in the Figure 9. Since in real conditions splices are usually protected with special sleeves, we also have investigated its influence on the integral emitted power. As a result, the reduction of 10-15% was observed and by taking this effect into account, one can derive that in real conditions external environment losses are $0.23 \pm 0.05$ of the total loss value on the given splice joint.

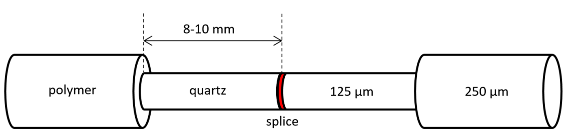


**Suppl Figure 9** | Schematic representation of a SM fiber splice joint without protection sleeve.

### Leaky modes

Since the splice connects two optical waveguides, then by applying the leaky modes theory, see Ref. [46] of the main text, to the ITU-T G.652.D single-mode fiber, the values of the propagation angle $\theta_z$ far from the core, e.g. near the quartz cladding's edge can be obtained for the first few $HE_{l+1,m}$ modes of the higher order, see Table 2.

All those values correspond to the case of total internal reflection from the quartz-air or polymer(acrylate)-air boundaries. However, emitted power was observed at distances of several centimeters after the splice joint during the experiments mentioned above, which means that this radiation could be scattered by some boundary defects. The illustration of this process is shown in Fig. 10. To prove this assumption, a piece of the fiber after the splice joint was visually observed with a microscope when transmitting red laser radiation through it (Fig. 11). One can see that there is a decrease in red light emission due to the good cleaning of quartz because pieces of mud, like cracks, are boundary defects too and consequently can lead to the escape of leaky modes from the waveguide. The integral value of emitted power, measured on the cleaned fiber right after the splice joint, was 5.74 nW or

$$3 \times 10^{-7} \text{ of the incident power } (P_{in} = 18 \text{ mW}).$$

Thus, with the polymer removal and good cleaning of the quartz, a significant decrease in the emitted power can be achieved. A further task is the implementation of this technique in real-life conditions where it is necessary to use fiber protection, which can potentially change the refractive indices difference and lead to the emission of the leaky modes into the external environment again.

| $l$, $m$ | $\tan\theta_z$ |
|---|---|
| 1, 1 | $9.88 \times 10^{-3}$ |
| 2, 1 | $8.33 \times 10^{-2}$ |
| 3, 1 | 0.14 |

**Suppl Table 2** | Results of leaky modes theory for the ITU-T G.652.D fiber.

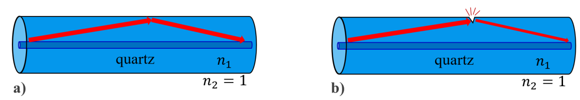


**Suppl Figure 10** | Schematic illustration of the: a) leaky mode reflection, b) leaky mode scattering into the external environment.

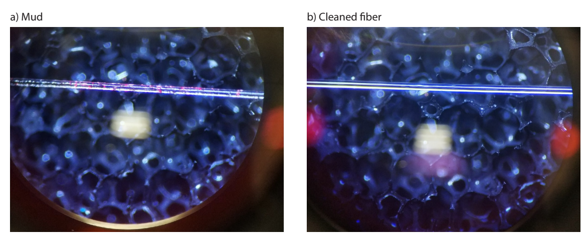


**Suppl Figure 11** | Observation of a 125 µm cladding under a microscope.

## NOTE 3. Used equipment

On the Alice side, the TLX1 Thorlabs laser is used to create laser radiation. Next, the iXblue MPZ-LN-10 phase modulator is in use for phase randomization of the generated laser radiation. Finally, the iXblue MXAN-LN-10 amplitude modulator is applied for intensity modulation. The signal coming from the FPGA to the amplitude modulator is amplified using the iXblue DR-VE-10-MO amplifier. On the Bob side, the Menlo Systems FPD610-FC-NIR detector is used to detect the optical signal. Then the analog signal from the detector is digitized by the Spectrum Devices M4i.2210-x8 ADC.

## NOTE 4. Temperature dependence

The optical loss control in the communication line enables not only determining the magnitude of the signal diverted by an eavesdropper but also the natural changes in the optical fiber transparency. One of the reasons for the transparency coefficient change is the temperature variations. Using the OTDR, we measure the losses magnitude change at the coil containing the 50 km of the fiber line upon the coil heating, see Fig. 12. The obtained reflectogram allows us to determine the loss magnitude of the whole segment of the optical fiber line from the slope of the log-log plot.

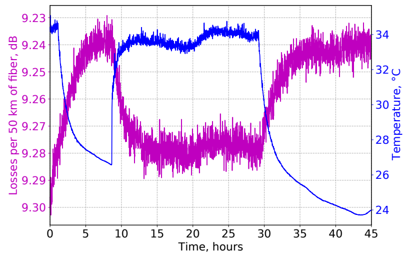


**Suppl Figure 12** | The time dependencies of the losses in the optical fiber and the fiber temperature. The temperature change is shown by the blue curve, the corresponding loss coefficient behavior is presented by the magenta one.

## NOTE 5. The narrowband filter

To reduce noise in the optical line it is necessary to suppress parasitic modes that do not carry information. For this purpose Terra Quantum AG has developed a special narrowband filter. Here in Fig. 13 we present the transmission spectrum of the narrowband filter having a bandwidth of 8.5 GHz with 3 dB dumping.

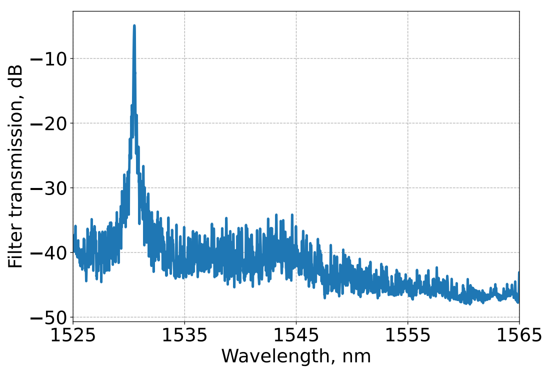


**Suppl Figure 13** | The dumping spectrum of the narrowband filter for the dumping of 3 dB.

## NOTE 6. Classical post-processing

Standard post-processing comprises three main stages: postselection, error correction and privacy amplification with each stage shown in Fig. 3 of the main text.We discuss the first two stages in detail in the Sec. 3 of the paper,while the specifics of the final stage are addressed below.

**Error correction**

For the purpose of correcting the resulting error, we utilize LDPC (linear-density-parity-check) code [4] practical realization. Usually, the input for such codes are probabilities of zero and one at each position of the raw key. Here, we deliver to LDPC only bit error rate $p_{\text{err}}$ averaged over the whole sequence. Bob estimates BER according to the their measurement results (see Fig. **??**(a). During error correction legitimate users disclose some information about the key to Eve depending on the syndrome's length. An accurate amount of the disclosed information is $f \cdot h_2(p_{\text{err}})$, where $f$ is the effectiveness.

**Privacy Amplification**

To increase the secrecy of the corrected key, it is necessary to compress it to such a size that Eve will have practically no information about it. Let $A$ and $B$ be the sets of adjusted sequences of length $m$ and final keys of length $n$, respectively. Then, to compress an element from the set $A$ into an element of the set $B$, we use the Toeplitz matrix $T$ of size $n \times m$, whose elements are random binary numbers. The set of Toeplitz matrices $T : A \longrightarrow B$ form the class of 2-universal hash functions $H \ni T$. According to the definition of Carter and Wegman [5] a class $H$ of hash functions from $A$ to $B$ is called 2-universal if there are at most $\frac{|H|}{|B|}$ hash functions $h \in H$ such that $h(a_1) = h(a_2)$ for any $a_1 \neq a_2 \in A$. In the paper [6], the 2-universality of Boolean matrices was shown, of which binary Toeplitz matrices are a special case. For $|H| = 2^{m+n-1}$ and $|B| = 2^n$ collision probability $P_{\text{collision}} = \frac{|H|/|B|}{|H|} = \frac{1}{|B|} = 2^{-n}$. Therefore, the longer the final key, the less chance of a collision. In real conditions, we compress keys in portions of at least a thousand bits.

## Suppl References

1. Predehl, K. *et al.*, A 920-kilometer optical fiber link for frequency metrology at the 19th decimal place. *Science* **336**, 441–444 (2012).
2. Droste, S. *et al.*, Optical-frequency transfer over a single-span 1840 km fiber link. *Phys. Rev. Lett.* **111**, 110801 (2012).
3. Chen, J. *et al.*, Quantum key distribution over 658 km fiber with distributed vibration sensing. *Phys. Rev. Lett.* **128**, 180502 (2022).
4. MacKay, D. J. C., Information Theory, Inference and Learning Algorithms. *Cambridge: Cambridge University Press)*, 2003.
5. Carter, J. L. and Wegman, M. N. Universal classes of hash functions. *Proceedings of the ninth annual ACM symposium on Theory of computing* 106 – 112 (1977).
6. Mansour, Y., Nisan, N., and Tiwari, P. The computational complexity of universal hashing. *Proceedings of the twenty-second annual ACM symposium on Theory of Computing* 235 – 243 (1990).